Jet-like flow and thrust from a flexible flapping foil in stationary fluid

Prof. Jaywant H. Arakeri and Sachin Y. Shinde
Department of Mechanical Engg.,
Indian Institute of Science, Bangalore-560012,
India.

Abstract: This study is an attempt to understand the flow produced by a hovering bird or by a fish when it starts suddenly in stationary water; the way it accelerates and develops thrust. Major focus is on the role of flexibility of the flapping foil or wing in these issues. A flexible flap with negligible mass and stiffness is attached at the trailing edge of a symmetric airfoil. The airfoil oscillates sinusoidally at a fixed location in stationary water. The wake flow generated by two airfoil models, one with flexible flap and the other with rigid trailing edge, are compared; the former produces narrow, coherent, self-similar jet-like flow nearly along the mean-position of model, on contrary to the quite divergent, meandering flow produced by rigid trailing edge airfoil. Comparison suggests that the flap plays a prominent role in defining the wake signature. Various aspects of flap motion and its flexibility in relation with the flow development are identified. Flexible trailing edge induces multiple vortices along with large vortices arranged in 'reverse Karman vortex street.' Flap accelerates the near-wake flow. It sheds the vortices with appropriate spacing and also imparts them convective velocity. Circulations around the vortices shed from flap do not increase linearly with increase in the chord. Airfoil with flap is found to be quite robust for amplitude-frequency variation.

1 Introduction

The pedantic definition of 'hovering' suggests that the mean force produced by the wings is exactly vertical and precisely balances the weight of the creature [8] while Rayner defines hovering as the mode of flight in which the body is at rest relative to undisturbed air, with the wake vertically beneath the animal, and with all fluid motions induced by the beating wings [24]. To achieve this, it has to counter the gravity, although it is relieved from the act of generating thrust necessary to propel forward. The animal tunes its wing-flapping kinematics such that thus produced force will be just enough to counterbalance its weight acting vertically downward, enabling the bird to hold the desired position. To fly or hover, momentum needs to be imparted to the surrounding fluid which they do in the form of vortices and obtain the desired forces by reaction. Hovering is a regular activity for insects, but for birds, it is "once-in-a-while" affair. So insects have been extensively studied to delve

Report Documentation Page

Form Approved
OMB No. 0704-0188

1. REPORT DATE	2. REPORT TYPE	3. DATES COVERED
29 DEC 2009	**FInal**	**01-08-2008 to 31-07-2009**

4. TITLE AND SUBTITLE	5a. CONTRACT NUMBER
Effect of Flexibility on Flapping Propulsion	**FA23860814106**
	5b. GRANT NUMBER
	5c. PROGRAM ELEMENT NUMBER
6. AUTHOR(S)	5d. PROJECT NUMBER
Jaywant H Arakeri	5e. TASK NUMBER
	5f. WORK UNIT NUMBER
7. PERFORMING ORGANIZATION NAME(S) AND ADDRESS(ES)	8. PERFORMING ORGANIZATION REPORT NUMBER
Indian Institute of Science,Indian Institute of Science,Bangalore 560012,India,IN,560012	**N/A**
9. SPONSORING/MONITORING AGENCY NAME(S) AND ADDRESS(ES)	10. SPONSOR/MONITOR'S ACRONYM(S)
AOARD, UNIT 45002, APO, AP, 96337-5002	**AOARD**
	11. SPONSOR/MONITOR'S REPORT NUMBER(S)
	AOARD-084106

12. DISTRIBUTION/AVAILABILITY STATEMENT

Approved for public release; distribution unlimited

13. SUPPLEMENTARY NOTES

14. ABSTRACT

Many lifting and propulsive surfaces in Nature are structurally flexible. How important is this flexibility on the lift and thrust forces generated and on the efficiency is an important and open question. The objective of the present work is to study some aspects of the unsteady flow associated with flapping flexible foils. The present research aims to experimentally study the effect of chordwise flexibility on the flow past a flexible flapping foil.

15. SUBJECT TERMS

Micro Air Vehicles (MAVs), Micro Air Vehicles (MAVs), Flight Control, bio-inspired flights

16. SECURITY CLASSIFICATION OF:			17. LIMITATION OF ABSTRACT	18. NUMBER OF PAGES	19a. NAME OF RESPONSIBLE PERSON
a. REPORT	b. ABSTRACT	c. THIS PAGE			
unclassified	**unclassified**	**unclassified**	**Same as Report (SAR)**	**18**	

deeper for the understanding of hovering flight. A crucial distinction between insect and bird flight is that the very small length scales involved in inset flight push them in laminar flow regime whereas almost all of the birds fly in turbulent regime, generally [11].

Three types of hovering are identified depending upon the angle made by the stroke-plane with the horizontal. The first type, usually known as 'normal hovering' in which the stroke plane is nearly horizontal. It is used by many insects and also by the hummingbird [11]. The second type in which the stroke plane is inclined and makes an angle between 30^o to 60^o with the horizontal is known as 'avian hovering'; e.g. Dragonfly. In third type the stroke plane is almost vertical; Ex. Large cabbage white butterfly. The lift generation takes place either by circulation or profile drag or combination of both. The first two types employ the former method while the animals hovering in the third type rely on the later method [7]. For the later two methods, the force is mainly generated during the downstroke while the upstroke produces very little or no force. Normal hovering mode generates nearly equal force in both the strokes. As opposed to the insects, the hummingbird does not contribute equally to support the weight during both halves of the wing-beat cycle though the motion looks kinematically similar, instead 75% of the weight support comes during the downstroke and 25% during upstroke [31].

The unusually high lift coefficients generated during hovering are quite puzzling and steady as well as quasi-steady aerodynamics theories are insufficient to explain them. Researchers found that hovering animals employ unsteady aerodynamic mechanisms. Wang [30] and Maxworthy [21] reviewed the unsteady aerodynamic mechanisms during the steady forward flight, gliding and hovering. A review [25] describes the fundamental aerodynamic principles lying behind the insect flight, stressing especially on the unsteady mechanisms involved towards the refinement of the existing quasi-steady model. Sane and Dickinson improved the existing quasi-steady model by adding the wing rotation effect [26]. Amongst the known unsteady mechanisms, some are: clap and fling mechanisms, delayed stall, vortex shedding from leading edge, wing rotation, rotational circulation, phase adjustment between wing rotation and translation, wake capture, flexibility of wings, etc. While mimicking the Dorsophila that hover in normal mode, with robofly, Dickinson *et. al.* found that the high lift coefficients are generated by three distinct and yet interactive mechanisms: delayed stall during translation phase while rotational circulation and wake capture generate forces during the stroke reversals. The phase difference between wing rotation and translation is also influential in force generation and maneuvering [6]. But the lift enhancement due to these unsteady effects is accompanied with increase in drag [30]. Weis-Fogh [32] suggested a novel mechanism of lift generation known as 'clap and fling' for hovering insects wherein the lift is quickly generated bypassing the Wagner effect [28]. Aerodynamic analysis by Lighthill [20] suggested that the viscous effects and the finite span of the wings result into the shedding of vortex rings below the hovering animal, thus supporting the weight by transforming the momentum to the fluid which takes the form of a jet of air blowing down vertically be-

low the animal. Wang [29] obtained nearly similar lift for a two-dimensional elliptic wing in hover as that of a three-dimensional wing, suggesting it essentially is not a three-dimensional phenomenon. Consideration of tip vortex modified the 'clap and fling' model [22].

To smaller or larger extent, flexibility is an ubiquitous property of the wings and fins of flying and swimming creatures. The wings and fins often deform, quite substantially sometimes, when they propel through air or water [5] and the deformed wing or fin profile plays key role in determining the flow around them, making the analysis even more profound. Due to deformation, the camber of the wing changes continuously and slight change in camber substantially affects the lift generated [1]. Existing literature reveals that very little has been contributed towards understanding the role of flexibility often found in the force generating appendages which are partially flexible, except a few studies [14, 15]. Nachtigall [23] suggests that among other mechanisms, the motion of flexible wings may also be one of the primary reason for the large lift generation during hovering [21]. The effect of wing flexibility during hovering has not been addressed to complete details due to the intricate fluid-structure interaction involved [25]. That makes it quite occult to understand analytically, how the wings deform, inertially or by fluid dynamic loading, or to find the exact contribution of either. Various aspects of wing flexibility have been addressed by Daniel and Combes [5]. The aerodynamic loading is quite small compared to the inertial-elastic forces for the wings whereas for the fins in water the fluid dynamic loading dominates the inertial force in deciding the fin deformation [5]. Wing venation in insect wings determines the flexural stiffness and its spatial distribution; spanwise and chordwise flexural stiffness scale respectively with cube of the wing span and square of the chord length [3, 4]. Zaho *et. al.* observed that wing venation along with wing flexibility is very important in force generation during insect flight [33].

Various methods have been used to analyze the hovering flight like unsteady actuator disk theory, jet-momentum approach, the vortex wake, etc. [24, 9, 10]. Ellington used vortex theory and modeled hovering with "pulsed actuator disk" that applies non-uniform pressure impulses to the air [10]. The flapping wing of hovering animal sheds continuously a vortex sheet in sympathy with the Kutta condition which later rolls-up forming the vortex rings. Rayner analytically modeled the wake generated from rest by a hovering animal with a chain of coaxial small-cored circular vortex rings stacked one upon other and constructed a model to predict the development of wake shape with time [24].

While many studies are available for thrust generation by flapping foils with forward velocity, very few studies similar to hovering have been conducted wherein the flapping foils are used to generate thrusts in stationary fluid. The ability of a sinusoidally plunging airfoil to produce thrust is known as the "Knoller-Betz effect". Knoller first observed this fact in 1909 and Betz in 1912, independently [18, 2]. Katzmayr observed this effect in a wind tunnel in 1922 [17], while Jones *et. al.* gave its experimental and numerical proof [16]. The dynamic stall vortices can be fully exploited to produce large thrust coefficients by an airfoil

in hovering and the hover jets can easily be vectored by adjusting the initial angle made by the airfoil chord with the horizontal, thus allowing easy transition from hovering to other modes of flight [12]. Lai and Platzer [19] observed the jet-like velocity profiles downstream of the airfoil plunging at zero freestream velocity and they were independent of the amplitude and frequency of oscillation when the velocity and lateral distance were non-dimensionalized by the maximum plunge velocity and amplitude of oscillation respectively. Heathcote *et. al.* [13, 14] studied the effect of airfoil flexibility; the moderate spanwise flexibility increases thrust as well as efficiency while there is an optimum chordwise flexibility for maximum thrust generation for a given plunge frequency and amplitude combination. The flow field was independent of amplitude-frequency variation for given flexibility. The downstream momentum flux gave the rough estimate of the thrust produced by the airfoil.

Another issue usually encountered in the thrust generating foils is the jet inclination, which is function of the initial conditions and random jet-switching which could be triggered even due to small disturbances, was reported earlier [16]. Lai and Platzer claimed the non-linear interaction of closely spaced vortices is responsible for jet inclination [19]. Heathcote and Gursul [15] showed that jet switching is quasiperiodic with period of switching two orders higher than the period of heaving and the switching frequency varies with heaving frequency and amplitude and inversely with airfoil stiffness. Jet switching diminishes with increasing Strouhal number, irrespective of airfoil stiffness.

The couplings between fluid and the flexible surfaces are not yet understood completely [34], so we approach this problem experimentally and focus to answer: How important is the flexibility often observed in the force generating flapping elements, in these issues? This paper investigates the effect of flexible surface appended at the rigid trailing edge on the flow over a symmetric airfoil pitching sinusoidally about a hinge point at 30% chord from the leading edge, fixed at a location in the stationary water, in an attempt to mimic the normal mode of hovering, usually observed in insects and hummingbird. The flexible flap performs combined heaving and pitching and traces the 'figure-of-eight' motion. To know the effect of flexibility and the difference it makes to the flow produced, we compare it with the flow over another airfoil without flap. The vortex wakes generated by the two airfoil models are studied in detail in a plane at the mid-span, qualitatively as well as quantitatively. The flows produced by them differ considerably conveying that the role of the flexible flap is not insignificant even though its mass and stiffness are! Flap kinematics is studied in relation with the flow generated. Parametric study is conducted by varying amplitude and frequency of oscillation.

Some of the probable applications where this study may prove to be useful are outlined here. The flow produced during the current experiments is nearly similar to that produced by a hand-fan in which its waving creates the breeze of air. This may be useful in designing a compact device that produces a jet of fluid by simple mechanical oscillations of the flexible flap, towards the replacement for the fan in electronic cooling applications. Piezoelectric fan

is used for the similar purpose where the leading edge vortices are used to create the flow. Though in this paper, we are not dealing with the analysis of unsteady flow produced in the very beginning i.e. as soon as the flow commences during the current experiments, such study will provide some insight in understanding the force generation mechanism employed by the fish when it suddenly accelerates and starts to move from rest in still water-an activity at the beginning of the steady swimming and also during unsteady swimming, common in maneuvering activities like catching prays and escape responses.

2 Experiments

The experiments are conducted in stationary water in a glass tank (800 mm X 800 mm X 350 mm). The airfoil-edges in spanwise direction are placed more than two chords away from water surface and bottom wall of glass tank. The model is confined between two end-plates with a gap of about 1 mm on either sides as shown schematically in Fig. 1, to keep the flow two-dimensional. Bottom end-plate is made of glass to provide optical access; top end-plate is of Aluminium. A servo motor oscillates the airfoil model sinusoidally about a pitching point at 30% chord from the leading edge. The desired motion is prescribed as,

$$\theta = \theta_{max} sin(2\pi f t), \tag{1}$$

where, 'θ' is the pitching angle, 't' is time, 'θ_{max}' and 'f' are respectively amplitude and frequency of oscillation.

It is a Panasonic A series AC motor (model: RAMA3AZA1E), 30 W, 2500 ppr incremental encoder controlled by a closed loop servo control mechanism. The driver is a Panasonic digital AC servo drive (model: MSDA3A3A1A, Type 1) 30 W, 220 V, single phase input with digital and analog command interfaces. The controller card is DMC-1425, two axis card from Galil Motion Controls.

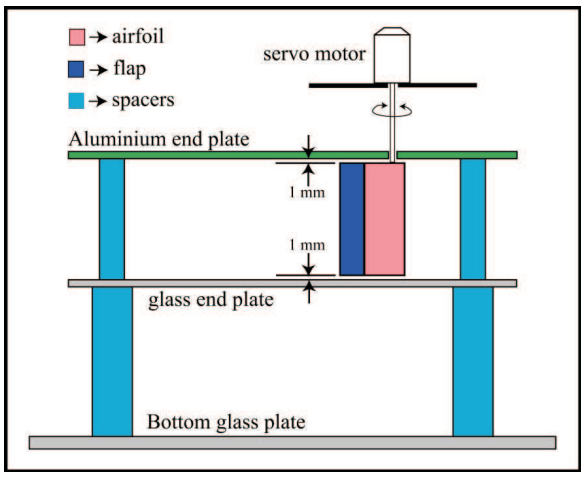

Figure 1: Schematic of the experimental set-up.

The experiments are conducted with two airfoil models (see Fig. 2): one with flexible trailing edge is termed as **model-F** and the other with rigid trailing edge is known as **model-R**. We fabricated the airfoil using the *'vacuum casting technique'*. The airfoil is made from a plastic material, ABS (Acrylonytril Butadyne Sulphide) whose density is 1.01 gm/cc, close to water density. The airfoil section is NACA0015 symmetric profile with chord of the rigid portion 40 mm and span 100 mm; maximum thickness is 6 mm at 30% of rigid chord from the leading edge. We extend the airfoil chord line beyond rigid trailing edge by appending a flexible flap made from 0.05 mm thick Polythene sheet which has negligible mass and stiffness. Its Young's modulus (E) is 3.02 x 10^8 N/m^2 and flexural rigidity (EI) is 3.15 x 10^{-7} N-m^2. It is inserted in a 0.1 mm wide slot, that protrudes inside the airfoil section for 10 mm, and provided along whole span at sharp trailing edge of airfoil (see Fig. 2(c)). The flap exposed to the fluid is 30 mm along the chord and 100 mm along the span. Thus the flexible chord is 75% of the rigid chord. To trace the flap, it is blackened in the plane of visualization except near the trailing edge portion to identify it. Airfoil is provided with two dye injection holes which open up on the surface at the maximum thickness location. Model-R, the airfoil with rigid, sharp trailing edge shown in Fig. 2(b) is exactly identical as model-F except that there is no flap at the trailing edge.

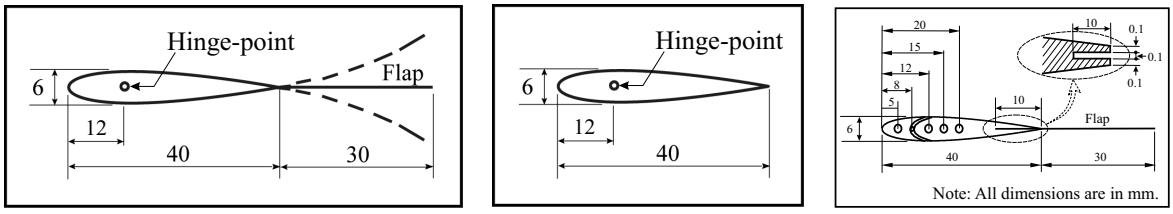

(a) (b) (c)

Figure 2: Schematic sectional views of the airfoil models: (a) model-F, (b) model-R, (c) details of model-F. All dimensions are in mm.

The flow is studied, qualitatively from the dye and particle visualizations and quantitatively from the particle image velocimetry (PIV) data, in a horizontal plane located in the middle along the airfoil span which is illuminated by a laser sheet. The optical arrangement is shown schematically in Fig. 3. The laser beam, directed through the front-coated mirrors, is converted into a horizontal sheet using a combination of plano-concave cylindrical lenses along with a plano-convex spherical lens. We captured the images with a CCD camera. The distance below the glass tank was not sufficient to focus the camera. So the optical path is broken and the visualizations are captured through a flat viewing mirror put below the tank. Camera unit comprises of a camera, computer, television-set and processor. We chose the field-of-view of about 200 mm x 150 mm for all experiments which varies to some extent from experiment to experiment.

For flow visualization, we use a continuous laser operating at up to 4 W at 488 nm (model: Spectra-Physics, Stabilite 2017). The visualizations are captured through Kodak

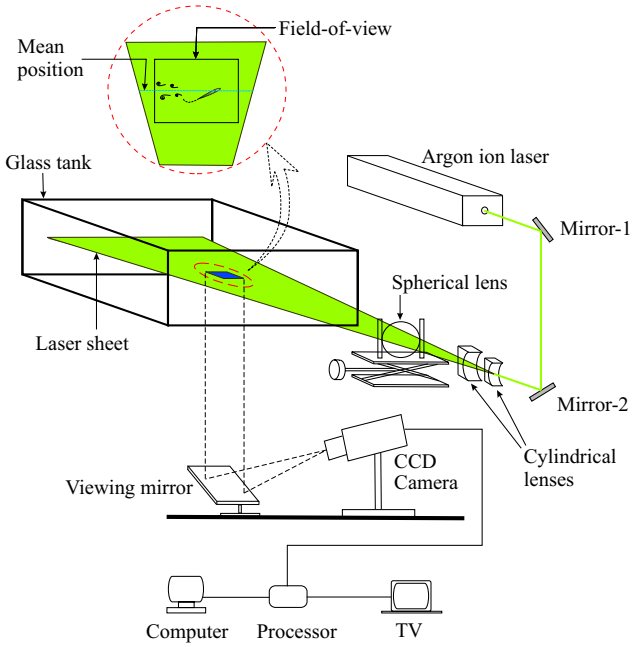

Figure 3: Schematic illustrating optics arrangement.

motion analyzer camera and Sony camcorder. We conduct dye visualizations with fluorescein Sodium salt and particle visualizations with Polystyrene particles of 75-100 μm diameter. To track the flap and airfoil, we employ shadow technique and image processing; in this, the shadow of the airfoil and flap is casted. Airfoil and flap locations are obtained by processing the images. The error introduced during clicking and picking the locations is about 1 to 2 pixels which corresponds to about 0.15 to 0.30 mm. Leading edge is difficult to capture for part of the half cycle since it goes into the shadow of the airfoil itself.

The velocity measurements are carried out with particle image velocimetry (PIV). In our experiments, the near-wake flow is two-dimensional, so the out-of-plane motion is negligible there. Hollow glass spheres of 30 μm size have been used as tracer particles. We use a Nd:YAG pulsed laser with double exposure (model: Big Sky Laser Quantel, ULTRA CFR Nd:YAG laser) which generates 120 mJ of energy in a pulse-width of 8 ns. The images are acquired using SharpVISION fire-wire camera (model: 1400-DE) synchronized with pulsed laser firing which is controlled through a computer. All images spanning the field-of-view have a resolution of 1360 x 1036 pixels with 80 x 60 grid nodes in X and Y directions respectively. We process the images through IDT proVISION-XS software to calculate velocities. We use 32 x 32 pixels interrogation window size with nearly 50% overlap to obtain velocities at all grid nodes. Vorticity is calculated using a subroutine provided in the software. We do the data post-processing and image processing in MATLAB 6.0.

The parameters varied during the experiments were amplitude and frequency of flapping. The stall angle for the static airfoil case is about 14^0. We choose three amplitudes of oscillation, 10^0 at which there is no static stall, 15^0 which is close to the stall angle and 20^0 where the flow may separate on the airfoil; and four frequencies for each amplitude, 1, 2, 3

and 4 Hz. In all, we collect data for 12 sets of parameters listed in Table 1. In this paper, we present a detailed analysis for **Set-VI**, *i.e.* amplitude of oscillation 15^0 and frequency 2 Hz. Except otherwise stated, all the data presented in this paper corresponds to Set-VI.

Set	**I**	**II**	**III**	**IV**	**V**	**VI**	**VII**	**VIII**	**IX**	**X**	**XI**	**XII**
amplitude (θ_{max})	10^0				**15^0**				20^0			
frequency (Hz)	1	2	3	4	1	**2**	3	4	1	2	3	4

Table 1: Values of the parameters used in the experiments.

3 The mean flow

Sinusoidal flapping of the airfoil with the flap in quiescent fluid creates a coherent, undulating jet composed of staggered vortices in the form of a 'reverse Karman vortex street'. Figure 4 shows an ensemble average of the measured velocity and vorticity fields at one phase during the oscillation cycle when the airfoil trailing edge is at the bottom-extreme location. Although the jet seen in the mean velocity field appears to move nearly along the mean-position in the downstream direction, the ensemble averaged flow shows jet-meandering about it to a little extent. Dye visualization shows (Fig. 5) a chain of smaller vortices, along with two relatively large counter-rotating vortices in each cycle. These smaller vortices are not captured in the PIV data due to insufficient resolution. Vorticity plot of the mean flow field in Fig. 6 shows a different view. Two strong counter-rotating vortices draw in and accelerate the fluid. The centers of these vortices are near the flap region. The shear layers of the jet portion show up as two long tongues of vorticity of either sign.

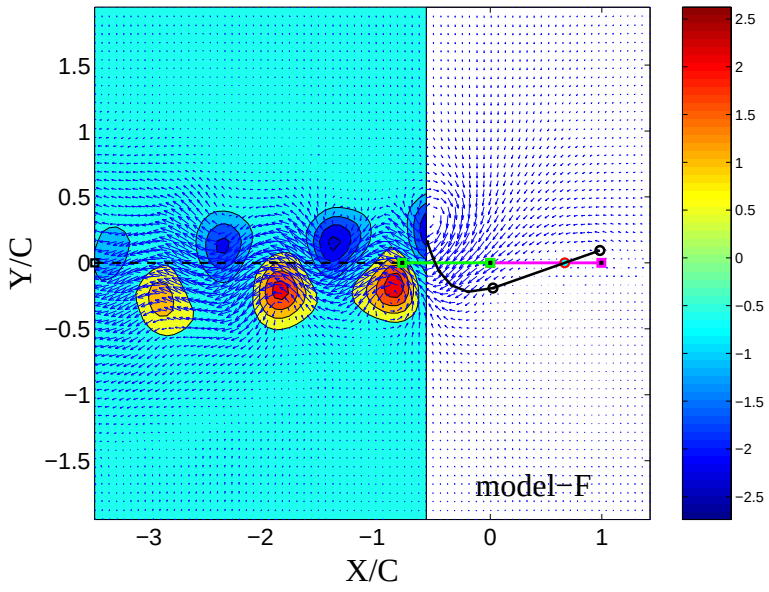

Figure 4: Ensemble average velocity and vorticity field when the rigid trailing edge is at bottom-extreme location: model-F.

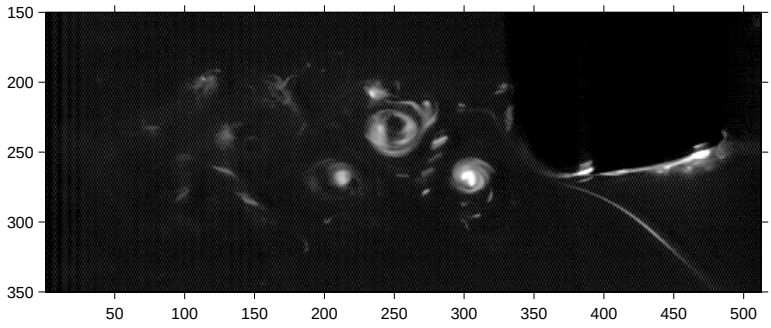

Figure 5: Dye visualization when the rigid trailing edge is at bottom-extreme location: model-F.

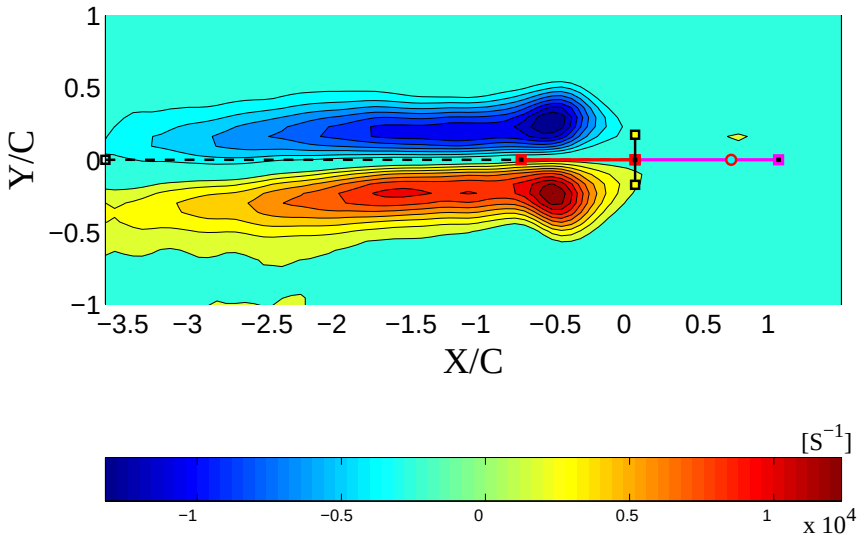

Figure 6: Average vorticity from mean flow field: model-F.

The suction of the quiescent ambient fluid and its acceleration to form a coherent jet are clearly seen in Fig. 7 which shows the iso-contours of velocity in X-direction. Such flow behavior is explained in Sec. 4. Jet-widening due to entrainment with the downstream distance is observed.

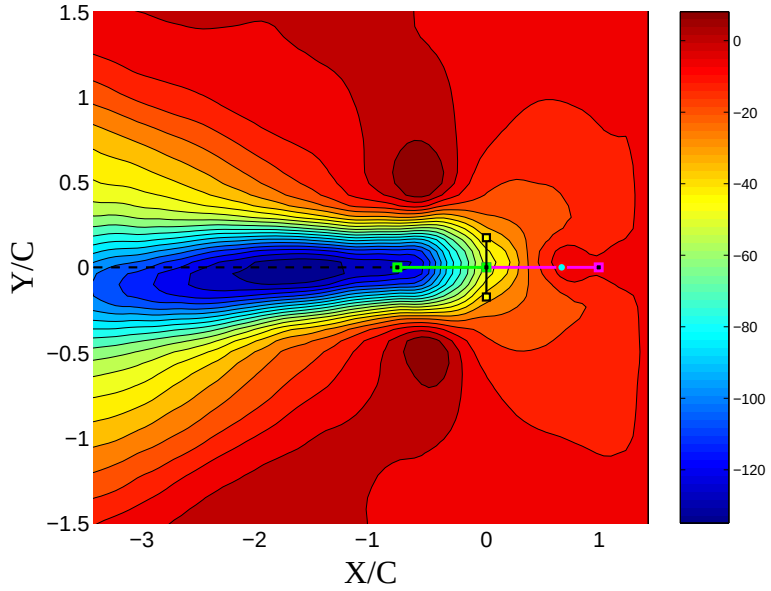

Figure 7: Iso-contours of velocity in X-direction (u) : model-F.

The variation in magnitude of u_{max} and the jet half-width with the downstream distance are also plotted in Fig. 8. The entire flow domain is usefully divided into different zones in X-direction as marked over the figure. The maximum u-velocity shows a sudden increase in zone-u2 that starts from near the mid-chord location of airfoil up to nearly three-quarters chord distance downstream of the rigid trailing edge; this is the active-flapping region where

work is done and momentum is added to the fluid. u_{max} shows steady and very small growth in zone-u3 (from -0.75C to -1.25C). It shows a rapid increase in zone-u4 i.e. beyond -1.25C. The highest u_{max}, which is 136 mm/S, is attained at 1.61 chords downstream of the rigid trailing edge and close to the mean-position line. Beyond this in zone-u5, a steady and fairly gradual fall in u_{max} is observed.

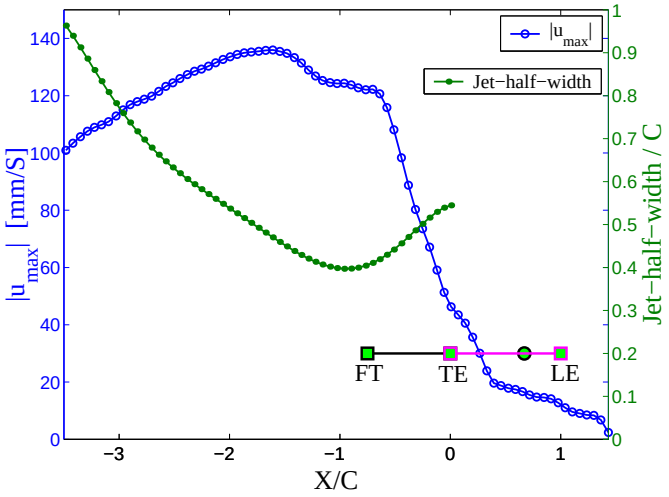

Figure 8: Variation of the maximum u-velocity and jet half-width in the downstream direction.

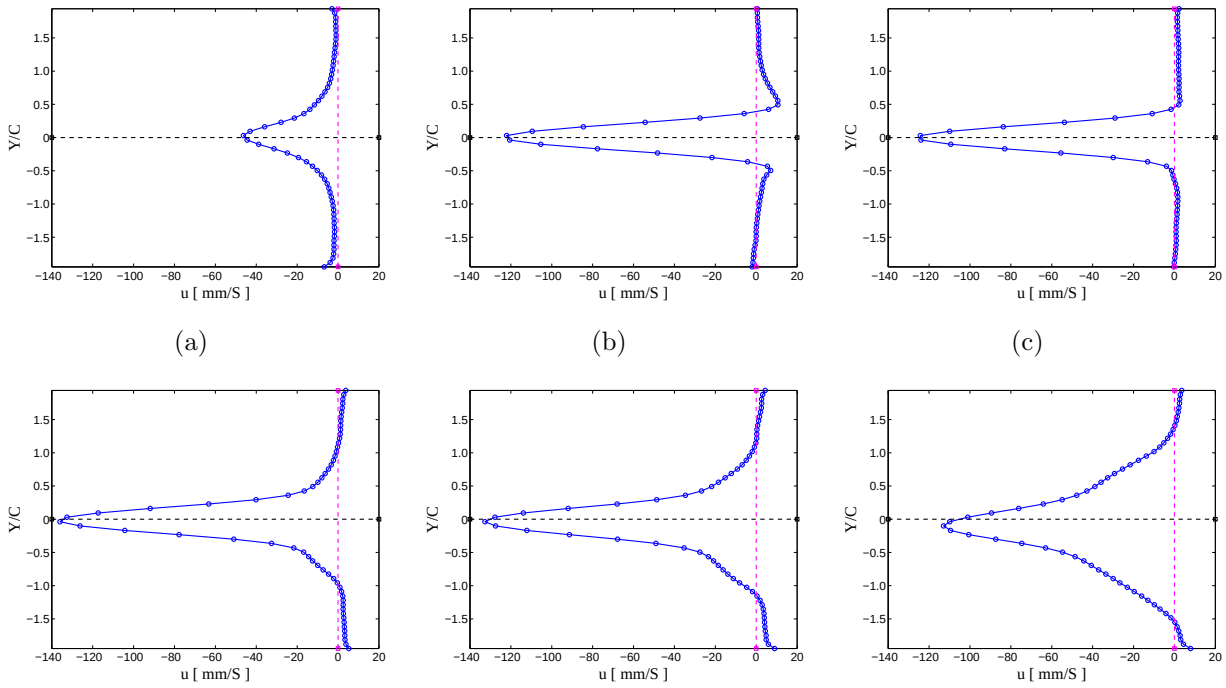

Figure 9: u-velocity profiles at some specific downstream locations; model-F: (a) $\frac{X}{C} \approx 0$, at trailing edge (b) $\frac{X}{C} \approx -0.76$, close to flap tip location in mean-position, (c) $\frac{X}{C} \approx -1$, (d) $\frac{X}{C} \approx -1.61$, highest u_{max} location, (e) $\frac{X}{C} \approx -2$, (f) $\frac{X}{C} \approx -3$.

The profiles of mean u (Fig. 9) at different X-locations show near Gaussian variation except at the edges. The fluid flowing with high u-velocity is confined mostly within a region spanning half chord above and below the mean-position. It is observed from Figures 8 and 9 that u increases in downstream direction, even beyond the flap region, for certain distance; this increase is explained by the actuator disk theory in Sec. 4.

The initial narrowing of the jet width is associated with the accelerating flow. Up to two and half chords, the flow is still under the effect of the favorable pressure gradient created near the flap region (see Sec. 4), so the jet grows gradually. Beyond this location, the jet grows more rapidly due to entrainment of ambient fluid. Jet-width is nearly one chord at downstream distance of three and half chords.

4 Accelerating flow: actuator disk theory

Figure 11 shows the streamlines, and pressure and velocity variations along the centerline for an ideal actuator disk; axial momentum flux variation will be same as that of axial velocity. A pressure jump across the disk produces favorable pressure gradients and accelerating flow both upstream and downstream of the disk. Momentum increase is ΔPA and rate of work done by the disk is equal to $(\Delta PA)\frac{u}{2}$.

The variation of mean momentum in X-direction for the flapping foil experiment (Fig. 10) is similar to that for an idealized actuator disk. The fluid momentum increases slowly in the airfoil region (zones m1 and m2) and rapidly in zone-m3 where the flap actively flaps. It then increases slowly in zone-m4, rapidly in zone-m5 and gradually in zone-m6. mom_X remains nearly constant thereafter, but with very small fluctuations.

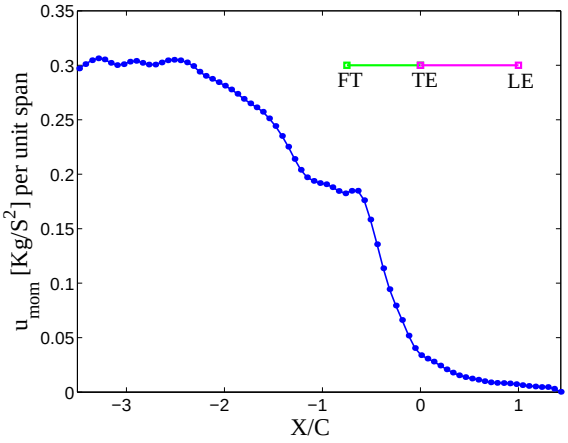

Figure 10: Variation of mom_X in downstream direction for model-F.

In the region between -1.75C to -2.5C, u_{max} keeps reducing (Fig. 8) while mom_X increases (Fig. 10). The jet widening with more fluid entrainment and effectiveness of the favorable pressure gradient generated near the model in increasing the velocity of entrained

fluid, explain this flow behavior.

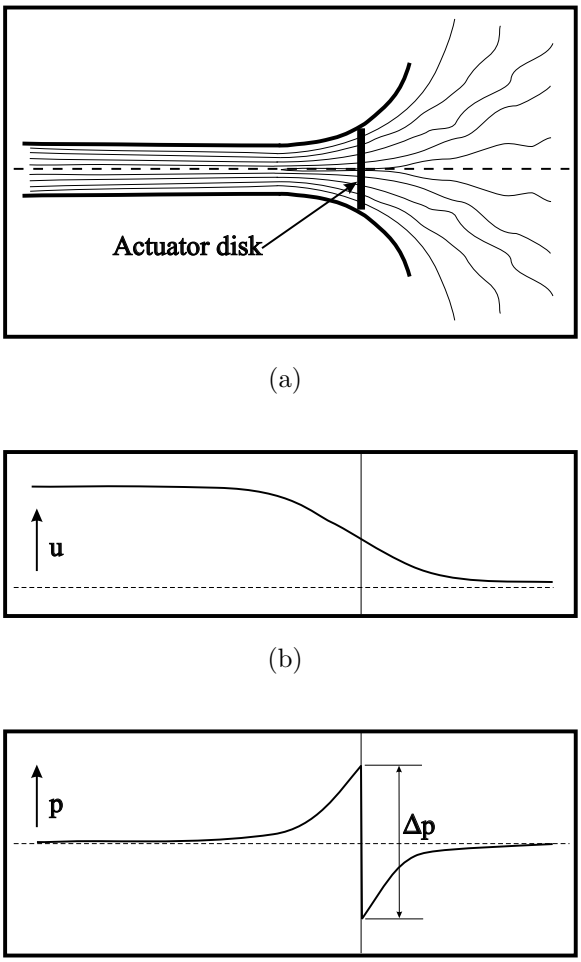

Figure 11: Schematic of the ideal actuator disk: (a) the flow, (b) velocity, (c) pressure.

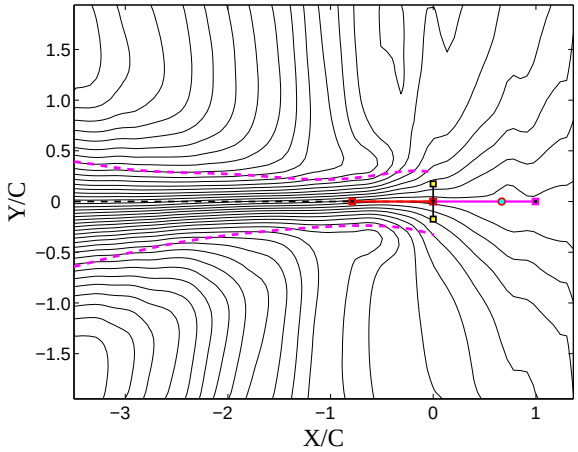

Figure 12: Streamlines around model-F, from the mean flow field. The dotted lines above and below the mean-position line indicate the jet-envelopes.

The accelerating flow observed in the immediate downstream (up to two and half

chords downstream from rigid trailing edge) of model-F, where the increase in momentum as well as velocity (up to 1.6 chords downstream; see. Figures 8 and 9) in downstream direction is observed, can be explained by the actuator disk theory. The remaining flow domain, where the momentum stays nearly constant, can be modeled like a jet.

Streamlines from the mean flow field plotted in Fig. 12 show that the mean flow generated by model-F resembles to the one produced by an actuator disk. There are some differences between an ideal actuator disk and model-F. First, in the idealized case velocity in the far downstream region and the mass flux remain constants. In contrast, due to entrainment, mass flux increases and centerline velocity decreases beyond about $\frac{X}{C} = -1.6$; in this region flow is similar to that in a two-dimensional submerged jet. Till about $\frac{X}{C} = -2.5$ momentum increases due to the favorable pressure gradient, though entrainment is present.

The other difference come from the fact in the idealized case actuator disk is an infinitesimally thin disk and the flow is steady, whereas in the flapping foil case pressure increase would be over a finite distance and the flow is periodic in time due to the sinusoidal pitching of the foil. Hence the pitching airfoil with the flexible flap may be more suitably modeled as an "unsteady actuator disk", in which, the pressure jump and the velocity in the slipstream are the functions of time. The pressure difference which draws in fluid and pushes it out is created by the flap motion. When the model oscillates, the flap bends considerably and its major portion keeps pushing the fluid in downstream direction, for most of the time over a cycle. A higher pressure would exist on the side of the flap which is pushing the fluid whereas its other side would experience pressure reduction at the same time. Thus, pushing action of the flap is the main cause for the speculated sudden pressure rise around the flap region.

5 Conclusions

We studied, qualitatively and quantitatively, the flow generated by two airfoil models, one with flexible trailing edge i.e. model-F and the other with rigid trailing edge i.e. model-R, when oscillated sinusoidally, at a fixed location, in stationary water. This study tries to identify the role of flexibility, often observed in the bird-wings and fish-tails, during the flow generation by a hovering bird or by a fish when it starts suddenly in stationary water; the way it accelerates and develops thrust. This is a simple method of flow generation in stationary fluid, in the sense that the jet and hence thrust is generated just by the mechanical oscillations of a flexible flap. Although, both the models produce jet-like downstream flow sustained mainly by the vortices, the flows differ in some terms. Addition of the flexible flap at the rigid trailing edge of airfoil produces more streamlined flow by pulling-in the fluid from sides, mainly in the flap region, and pushing it back than the airfoil without it. Airfoil with flexible flap produces a narrow, coherent, undulatory jet confined among the vortices arranged in 'reverse Karman vortex street', whereas the one without flap produces

quite widespread flow. The jet produced by model-F runs nearly along the mean-position with slight meandering; on the other hand, the jet produced by model-R meanders about the mean-position quite randomly and continuously. We attribute this jet meandering to the vortex-vortex interactions, their strengths, shedding pattern, spacing among them, etc. Interestingly, almost all the vorticity is confined within the narrow region around the mean-position in the wake of model-F whereas it is spread in the wake of model-R.

Some aspects of flap kinematics, studied in relation with the observed fluid flow, suggest that the flap alters the flow substantially and plays a prominent role in defining wake signature. Flap tip and trailing edge move almost in-phase in X-direction, but a phase difference of nearly 137^o exists in Y-direction; trailing edge leads the flap tip. The frequency of flap tip deflection in X-direction is double of that in Y-direction. Large flap deflections, and even second mode at some phases, are observed. Flap velocities higher than rigid trailing edge affect the vortex shedding pattern. While model-R mainly sheds large vortical structures, the flexible trailing edge sheds vortices of two kinds: smaller multiple vortices, shed in order to satisfy the Kutta condition at every instant, and the relatively bigger vortices. The larger vortex is the manifestation of 'stopping-vortex' developed during the direction-reversal of rigid airfoil portion which is strengthened and matured while moving over the flexible flap and shed by its tangential removal. The rigid airfoil portion plays the role of generating bigger vortices, whereas the flap, apart from shedding the smaller multiple vortices which may later merge in the bigger vortices strengthening them, enhances their strength, releases them at right places and imparts convective velocity due to which they and hence the jet-like flow are sustained far downstream. Some humps seen in the flap tip velocity plot in Y-direction and the non-identical flap tip acceleration and deceleration in X-direction when it travels both-ways might be the consequences of shedding bigger vortex. Moreover, it is shed predominantly only when the flap tip moves away from the rigid trailing edge. The jet-like flow is found to be stable, qualitatively, for the observed vortex aspect ratio (0.3584 for Set-VI).

Flap accelerates the flow in the near-wake region. We ascribe this to the favorable pressure gradient generated due to the sudden pressure difference developed by the flexibility and the pushing action of the flap, mainly near the flap region, which is explained by modeling the airfoil with flexible flap as an actuator disk. Momentum in downstream direction continues to increase even after u_{max}, which occurs nearly along the mean-position line, started to reduce, due to the entrainment causing increased fluid mass that accelerates simultaneously. Beyond two and half chords, the flow obeys characteristics of jet-like flow. Total chord of model-F is 75% more than model-R, but the circulation around vortices shed from model-F is more by a factor of about three than model-R which is a consequence of flexibility introduced by the flap. A point of zero velocity (POZV) exists over the flap portion when it deflects in second mode. It is considered as a movable hinge point which travels over the flap region resulting in differential flap portions, pulling and pushing the fluid about this

hinge point and thus enhancing the circulation shed, finally. The downstream flow, at least within the jet-width region, is found to be self-similar for the local u_{max} and jet-width.

The airfoil with flexible flap is found to be quite robust, qualitatively, for the amplitude-frequency variation since it produces nearly similar flow for all the parameter-sets studied.

References

[1] Batchelor, G. K., *An introduction to fluid dynamics*, Cambridge University Press, 1997.

[2] Betz, A., "Ein Beitrag zur Erklarung des Segelfluges," *Zeitschrift fur Flugtechnik und Motorluftschiffahrt*, vol. **3**, pp. 269–272, 1912.

[3] Combes, S. A. and Daniel, T. L., "Flexural stiffness in insect wings. I. Scaling and the influence of wing venation," *J. Exp. Biol.*, vol. **206**, pp. 2979–2987, 2003.

[4] Combes, S. A. and Daniel, T. L., "Flexural stiffness in insect wings. I. Spatial distribution and dynamic wing bending," *J. Exp. Biol.*, vol. **206**, pp. 2989–2997, 2003.

[5] Daniel, T. L. and Combes, S. A., "Flexible wings and fins: Bending by inertial or fluid-dynamic forces?," *Integr. Comp. Biol.*, vol. **42**, pp. 1044–1049, 2002.

[6] Dickinson, M. H., Lehmann, F. and Sane, S. P., "Wing rotation and aerodynamic basis of insect flight," *Science*, vol. **284**, pp. 1954–1960, 1999.

[7] Ellington, C. P., "The aerodynamics of hovering insect flight. I. The quasi-steady analysis," *Phil. Trans. R. Soc. Lond.*, vol. **B 305**, pp. 1–15, 1984.

[8] Ellington, C. P., "The aerodynamics of hovering insect flight. III. Kinematics," *Phil. Trans. R. Soc. Lond.*, vol. **B 305**, pp. 41–78, 1984.

[9] Ellington, C. P., "The aerodynamics of hovering insect flight. IV. Aerodynamic mechanisms," *Phil. Trans. R. Soc. Lond.*, vol. **B 305**, pp. 79–113, 1984.

[10] Ellington, C. P., "The aerodynamics of hovering insect flight. V. A vortex theory," *Phil. Trans. R. Soc. Lond.*, vol. **B 305**, pp. 115–144, 1984.

[11] Ellington, C. P., "Insects versus birds: the great divide," *AIAA paper*, vol. **35**, pp. 1–6, 2006.

[12] Freymuth, p., "Thrust generation by an airfoil in hover modes," *Exp. fluids*, vol. **9**, no. 1, pp. 17–24, 1990.

[13] Heathcote, S., Wang, Z. and Gursul, I., "Effect of spanwise flexibility on flapping wing propulsion," *J. Fluid Struct.*, vol. **24**, pp. 183–199, 2008.

[14] Heathcote, S., Martin, D. and Gursul, I., "Flexible flapping airfoil propulsion at zero freestream velocity," *AIAA J.*, vol. **42**, no. 11, pp. 2196–2204, 2004.

[15] Heathcote, S. and Gursul, I., "Jet switching phenomenon for a periodically plunging airfoil," *Phys. Fluids*, vol. **19**, pp. 0271041–02710412, 2007.

[16] Jones, K. D., Dohring, C. M. and Platzer, M. F., "Experimental and computational investigation of the Knoller-Betz effect," *AIAA J.*, vol. **36**, no. 7, pp. 1240–1246, 1998.

[17] Katzmayr, R., "Effect of periodic changes of angle of attack on behaviour of airfoils," NACA Rept. 147, Oct. 1922 (translated from *Zeitschrift fur Flugtechnik und Motorluftschiffahrt*, March 31, 1922, pp. 80–82, and April 13, 1922, pp. 95–101).

[18] Knoller, R., "Die Gesetze des Luftwiderstandes," *Flung- und Motortechnik(Wien)*, vol. **3**, no. 21, pp. 1–7, 1909.

[19] Lai, J. C. S. and Platzer, M., F., "Characteristics of a plunging airfoil at zero freestream velocity," *AIAA J.*, vol. **39**, no. 3, pp. 531–534, 2001.

[20] Lighthill, M. J., "On the Weis-Fogh mechanism of lift generation," *J. Fluid Mech.*, vol. **60**, part 1, pp. 1–17, 1973.

[21] Maxworthy, T., "The fluid dynamics of insect flight," *Annu. Rev. Fluid Mech.*, vol. **13**, pp. 329–350, 1981.

[22] Maxworthy, T., "Experiments on the Weis-Fogh mechanism of lift generation by insects in hovering flight. Part 1. Dynamics of the 'fling'," *J. Fluid Mech.*, vol. **93**, part 1, pp. 47–63, 1979.

[23] Nachtigall, W., "Rasche Richtungsanderung und Torsionen schwingender Fliegenflugel und Hypothesen uber zugeordnete instationare Stromungseffekte," *J. Comp. Physiol.*, vol. **133**, pp. 351–355, 1979.

[24] Rayner, J. M. V., "A vortex theory of animal flight. Part 1. The vortex wake of a hovering animal," *J. Fluid Mech.*, vol. **91**, part 4, pp. 697–730, 1979.

[25] Sane, S. P., "The aerodynamics of insect flight," *J. Exp. Biol.*, vol. **206**, pp. 4191–4208, 2003.

[26] Sane, S. P. and Dickinson, M. H., "The aerodynamic effects of wing rotation and a revised quasi-steady model of flapping flight," *J. Exp. Biol.*, vol. **205**, pp. 1087–1096, 2002.

[27] Taylor, G. I., "Formation of a vortex ring by giving an impulse to a circular disk and then dissolving it away," *J. App. Phys.*, vol. **24**, no. 1, pp. 104, 1953.

[28] Wagner H., "Uber die Entstehung des dynamischen Auftriebes von Tragflugeln," *Z. Angew. Math. Mech.*, vol. **5**, pp. 17–35, 1925.

[29] Wang. Z. J., "Two dimensional mechanism for insect hovering," *Phys. Rev. Lett.*, vol. **85**, no. 10, pp. 2216–2219, 2000.

[30] Wang, Z. J., "Dissecting insect flight," *Annu. Rev. Fluid Mech.*, vol. **37**, pp. 183–210, 2005.

[31] Warrick, D. R., Tobalske, B. W. and Powers, D. R., "Aerodynamics of the hovering hummingbird," *Nature*, vol. **435**, pp. 1094–1097, 2005.

[32] Weis-Fogh, T., "Quick estimates of flight fitness in hovering animals, including novel mechanisms for lift production," *J. Exp. Biol.*, vol. **59**, pp. 169–230, 1973.

[33] Zaho, L., Huang, Q., Deng, X. and Sane, S. P., "Aerodynamic effects of flexibility in flapping wings," *J. R. Soc. Interface*, published online on 19 August 2009, pp. 1–13, 2009.

[34] Zhang, J., Childress, S., Libchaber, A. and Shelley, M., "Flexible filaments in a flowing soap film as a model for one-dimensional flags in a two-dimensional wind," *Nature*, vol. **408**, pp. 835–839, 2000.